# Correlation of Measured soft x-ray pulses with modeled dynamics of the plasma focus

| | |
|---|---|
| Journal: | *IEEE Transactions on Plasma Science* |
| Manuscript ID: | Draft |
| Manuscript Type: | 10 Original Article (Other Topics in Plasma Science) |
| Date Submitted by the Author: | n/a |
| Complete List of Authors: | Lee, Sing; Institute for Plasma Focus Studies, Director<br>Saw, Sor Heoh; INTI International University, Pro Vice Chancellor<br>Lee, Paul; National Institute of Education, Natural Sciences and Science Education<br>Rawat, Rajdeep; National Institute of Education, Nanyang Technological University, NSSE<br>Abdou, Ali; Kansas State University, Mechanical and Nuclear Engineering<br>Talebitaher, Alireza; Nanyang Technological University, NIE<br>Chong, Perk Lin; INTI International University, Engineering<br>Roy, Federico; INTI International University, Engineering<br>Singh, Arwinder; INTI International University, Engineering<br>Wong, David; INTI International University, Engineering<br>Devi, Kavuri; INTI International University, Engineering |
| Key Words: | Plasma focus |
| Specialty/Area of Expertise: | Plasma Focus modelling, Neon soft x-rays, Soft x-ray measurements, Plasma focus dynamics |
| | |

# Correlation of Measured soft x-ray pulses with modeled dynamics of the plasma focus

S Lee[1,2,3], S H Saw[1,2], R S Rawat[3], P Lee[3], A.Talebitaher[3], A E Abdou[4], P L Chong[1], F Roy[1], A Singh[1], D Wong[1] and K Devi[1]

[1]INTI International University, 71800 Nilai, Malaysia
[2] Institute for Plasma Focus Studies, 32 Oakpark Drive, Chadstone, VIC3148, Australia
[3] National Institute of Education, Nanyang Technological University, Singapore 637616
4Kansas State University, Manhattan, KS 66506, USA

**The 6-phase Lee model code is used to fit the computed current waveform to the measured current waveform of INTI PF (2.2kJ at 12 kV), a T2 plasma focus device, operated as a source of neon SXR with optimum yield around 2 Torr of Neon. The characteristic He-like and H-like neon line soft x-ray (SXR) pulse is measured using a pair of SXR detectors with selected filters that by subtraction has a photon energy window of 900 to 1550eV covering the region of the characteristic neon SXR lines. From the analysis of the fitted current and the measured SXR pulses, the characteristic neon SXR pulses are correlated to the pinch dynamics; and the subsequent slightly harder SXR pulses are correlated to the anomalous resistance phase. The characteristic neon SXR yield is measured as 1.1 J; with a duration of 25 ns. The characteristic neon SXR typically starts 10 ns before the pinch phase and continues through the end of the 10 ns pinch phase, tailing into the anomalous resistance phase. Harder SXR pulses, probably Bremsstrahlung are correlated to the anomalous resistance phase, with the main pulse occurring some 200 ns after the characteristic neon SXR pulse.**

***Index Terms*—Plasma Focus modelling, Soft X-ray measurements, Plasma Focus Dynamics, Neon Soft X-rays**

## I. Introduction

The dynamics of the plasma focus (PF) computed from the Lee model code [1] is found to be in general agreement with experimental measurements when the computed current waveform is properly fitted to the measured current waveform [1-11]. The features in agreement include the temporal profiles of the axial and the radial speeds.

Recently it was found [12] that for modelling purposes plasma focus devices may be conveniently classified into T1 and T2; the former having low static inductance $L_0$ typically in the tens of nH whilst the latter typically having $L_0$ of more than 100nH.

The T1 plasma focus devices have measured current waveforms which are well fitted to the computed current waveforms using the standard 5-phase model code whereas T2 devices have a small computed 'regular' current dip (RD) which could only be fitted to the first part of the measured current dip. The measured current dip then continues beyond the computed dip (RD) into a longer and deeper extended dip (ED) which cannot be fitted using the 5-phase model code. The INTI PF is a typical T2 type plasma focus device. To complete the fit for T2 devices the 5-phase Lee Model code was extended to the 6-phase code with the addition of a post-pinch phase of anomalous resistances. With this new 6-phase code the computed current waveform is fitted very well to the measured current waveform (see Fig 1).

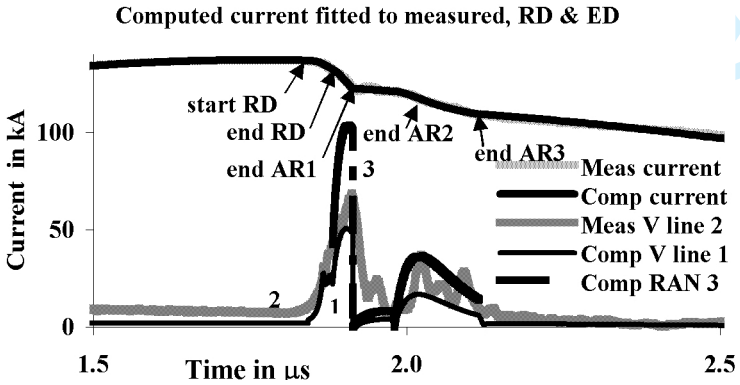


Fig 1 Fitting computed current waveform to measured current waveform for the KSU PF. The time scale is expanded in this figure and shows the radial phases only [12]. The standard 5-phase code provides a fit of the computed with the measured current waveform only up to the point 'end RD' as shown in the figure above. Beyond that point fitting of the computed to the measured requires the extension to a 6-phase code with the use of 3 anomalous resistances for the regions AR1, AR2 and AR3. Typically the fitting is so good that the computed and measured current traces overlap and appear as one trace (the top trace)

The question then arises: What is the correlation between the time history of the measured SXR pulse with the different phases of the computed current waveform which has been fitted to the measured current waveform? To answer this question entails the

fitting of the current waveform in the region of the RD to an accuracy of 4 ns or better since the phase of greatest interest, the pinch phase has a computed duration of around 10ns for the INTI PF [3]. This is to ensure that we get the time position of the SXR pulse relative to the pinch phase with a time resolution of 40% of the pinch phase duration.

For several applications we also need to differentiate the neon SXR into the characteristic He-like and H-like neon line radiation and the slightly harder SXR such as Bremsstrahlung emitted by hotter fully ionized neon plasmas. The characteristic radiation of the He-like and H-like neon consists of two dominant lines at 921 eV (13.447 Å) and 1020 eV (12.132 Å) contributing 80% of the characteristic neon SXR radiation. The remaining 20% comprises mixed lines and continuum radiation between 1070-1548 eV (8-11.568 Å) [13]. Since these characteristic He-like and H-like radiations are predominantly line radiation we shall apply the term characteristic He-like and H-like neon line radiation to the sum of these emissions in the photonic energy window of 900-1550 eV (8-13.5 Å). Differentiating the neon SXR into characteristic neon line emission and the harder continuum SXR and correlating these separately to the various phases of the focusing plasmas provide useful information on applications and on the modelling.

## II. THE METHOD

### IIa. The Experiment

We develop a method to reduce the electrical noise in the measured current waveform. A 7-turn Rogowski coil is used to record the rate of change of current dI/dt with the coil output connected to a DSO at a sample rate of 1 GSa/s at a frequency response of 200MHz. The signal is then numerically integrated [14]. This method is found to give a signal with good frequency response and also reasonably free of electrical noise in the form of coil self oscillations

The SXR pulses (from 2 detector channels of diode x-ray spectrometer DXS) and the corresponding measured current and voltage are taken together on a 4-channel Digital Storage Oscilloscope DSO. The voltage signal was obtained using a resistive divider. This divider had been tested and showed a time response in the region of 15 ns [15].

The absorption filters method based on foil absorbers and silicon PIN diode detectors is used in the SXR spectrometer [16]. The two SXR detectors of the DXS are used together as a differentially filtered pair, Ch1 and Ch2 of DXS, to measure the characteristic He-like and H-like neon line SXR by the method of subtraction [17]. Each detector consists of a reverse-biased BXP65 PIN photodiode with a wide spectral range. The glass window of the BPX65 detector is removed extending the spectral range and making the detector sensitive to SXR.

The foil filter of the first channel (Ch1) is designed so that Ch1 has the same sensitivity as the differently foil-filtered Ch2 over all wavelength range except in a window corresponding to the characteristic He-like and H-like neon line emission [16].
The characteristic He-like and H-like neon line emission and some small amounts of continuum had been measured as [13] :

| | | | |
|---|---|---|---|
| 921eV: | (13.447 Å) | 65% | region 1 (strong line) |
| 1020eV | (12.132Å) | 15% | region 2 (strong line) |
| 1548-1070 eV | (8-11.568Å) | 20% | region 3 (lines & continuum) |

Therefore the required window of sensitivity which Ch1 needs to have additional to its otherwise identical sensitivity profile with Ch2 is the spectral or photonic energy range of 900-1550 eV. In designing the required filter these emission wavelength with expected line intensities are suitably weighted and factored in [18] to obtain the average sensitivity factor for the relatively narrow spectral window of 900-1550 eV.

A suitable pair is designed as follows. The first detector is covered with 13 μm Al (SXR Ch1) whilst the second detector is covered with 3 um Al+125 μm mylar (SXR Ch2). Fig. 2 shows the sensitivities of each channel for this pair as a function of photon energy in eV. The sensitivity of each channel is obtained using the quantum detection efficiency [19] of silicon, x-ray transmission efficiency through neon gas at different pressure and fixed path length of the 25 cm between the anode tip and the detector and the x-ray attenuation length of solids [20]. The sensitivity curves are similar to the one shown in reference [17] as the filter materialsare the same though of slightly different thicknesses.

At the scale of Fig 2, the two sensitivity curves are identical and appear as one overlapped curve from 0-20,000 eV, except for the sharp spike on the left side of the curve with photonic energy range of 900-1550 eV. This spike (transmission window) belongs to Ch1 only.

The filter pair, for Ch1 and Ch2, is designed to give a difference window in the spectral region of the characteristic He-like and H-like SXR emission from neon 900-1550 eV [17]. Subtracting the signal of Ch2 from Ch1 thus allows the amount of characteristic neon SXR falling on the detectors to be computed. For example if for a shot the difference signal between the two channels is zero this means that no emission in the 900-1550 eV window is detected. This means that no characteristic neon SXR is detected. If there is a difference signal, it can only come from the 900-1550 eV window and the difference signal is a measure of the characteristic neon SXR detected. If pulses are detected by the channels but there is no difference signal, that means that each channel is detecting a signal with photon energy considerably above 1550 eV. That means that in that case SXR harder than the characteristic neon SXR emission are detected.

Thus capturing the SXR pulse on a DSO, the absolute amount of characteristic neon line SXR falling on the detector may be measured; and by assuming a point source radiating isotropically, the source yield can then be estimated by space integrating

over 4π ; and time integrating over the duration of the pulse. Both detectors have been normalized to one another and are positioned side by side with the same distance to the focus position where the focus pinch emits the radiation to be detected.

In this manner the experimentally measured current, tube voltage and characteristic neon SXR yield are time correlated and ready for comparison with the time variations of computed current and trajectories. SXR harder than the characteristic neon SXR are also time-correlated.

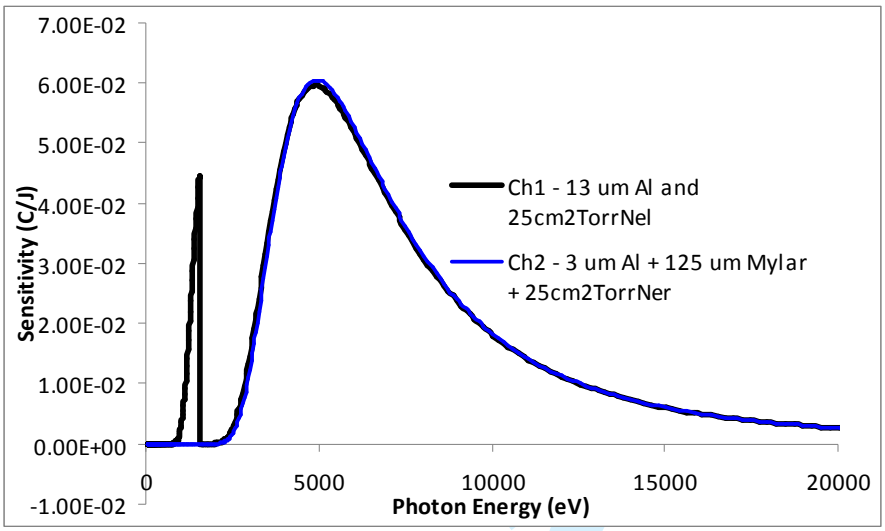


Fig 2 The sensitivity of the two channels. Ch1 and Ch2 are designed to have identical sensitivity curves for the region from around 1550 eV upwards to 20000 eV and beyond. The only difference in the two curves is that Ch1 has an additional region of sensitivity from 900 eV to 1550 eV (the spike-like feature between 0 and 2500 eV in the figure above belongs to Ch1 only). In the other spectral (or photon energy) regions there are two curves on top of each other, so the two curves are seen as one.

IIb. The Numerical Experiment

The INTI PF had its electrical parameters determined to be as follows: $L_0$=114 nH, $C_0$=30 μF, $r_0$=13 mΩ [21]; its tube parameters are: b=3.2 cm, a= 0.95 cm and $z_0$=16 cm. The code is configured accordingly.

The computed current is fitted to the measured current [1-11] in steps described below:
First the axial phase (see Fig 3 where the axial phase is from time=0 to the point indicated as 'start RD') is fitted by varying $f_m$ and $f_c$ and the 3 features of current rise slope, the topping profile and the peak value of current are the fitting indicators. To compensate for the non-instantaneous switching of the spark gap as compared to the modeled instantaneous switching a displacement in time is made to the computed current trace (relative to the measured trace). The critical topping region is expanded again and again as the fitting is fine-tuned until an accuracy of 2-4ns is typically achieved in the fitting of the computed to the measured current waveforms, particularly at the roll-over region (or the start of the dip in the current trace) where the apparent beginning of the dip occurs. The end of the axial phase (indicated in Fig 3 by the arrow 'start RD') actually occurs a little before this roll-over starts to become apparent.

Next the radial phase (regular dip RD) is fitted by adjusting the radial parameters $f_{mr}$ and $f_{cr}$. The features to observe for the fitting most critically is the slope of the dip. The traces are expanded in the radial phase until the fit of the slopes is obtained with confidence at the 2-4 ns level. At these high levels of expansion whilst the computed slope is being fitted it may be necessary also to make further really fine tuning to the axial $f_m$ to assist the fitting of the slope of the dip. The end result of this part of fitting is that the RD (from start to end) is fitted with sufficient accuracy to the first part of the measured current dip (the point end RD in Fig 3).

Next the computed current trace of the anomalous resistance regions [12] are fitted to the corresponding measured current trace one after the other. Typically the anomalous resistance (RAN) region is divided into 3 regions denoted RAN1, RAN2 and RAN3. We apply a resistance term to each of the 3 sections, the term being

$$R=R_0[exp(-t/t_2)-exp(-t/t_1)].$$

We adjust the parameters $R_0$, $t_2$ and $t_1$ for each of the section as well as a fraction (*endfraction*) which terminates the term. Region RAN1 is fitted first, the parameters that are varied for the fitting are: the amplitude $R_0$ of the anomalous resistance, the risetime $t_1$ and the falltime $t_2$ ; again expanding the traces until sufficient resolution is attained. When a satisfactory fit is obtained, then the next RAN2 region is fitted and so on for the RAN3 region.

As can be seen in Fig 3 and Fig 4, typically the fit between the computed current trace to the measured is so good that the two curves appear as one over almost the whole of the axial phase and all the radial phases up to the end of the anomalous resistance phases.

### IIc. Correlating the time history

We had already determined that at 12 kV the INTI PF achieves optimum characteristic neon line SXR at a pressure of 2 Torr. For the correlation work we fired the INTI PF at this operation point and obtained a discharge current waveform together with tube voltage and SXR Channel 1 (filtered with 13 μm Al and protected by a 3 μm film of mylar) and SXR Channel 2 (filtered with 3 μm Al and 125 μm mylar).

The measured SXR time profiles (2 channels) are plotted from the digital data already time-aligned to the measured time profile of current. The computed time profile of the current is fitted to the measured time profile of current, described in IIb above; thus time aligning the computed current profile to the measured current and hence to the SXR data. This computed current profile is computed in phases. Time markers (see Fig 4) for the start of the radial RD phase, the start and end of the pinch phase, and the RAN1, RAN2 and RAN3 phases are placed on the comparative chart. In this way the time period of the characteristic neon SXR and the subsequent harder SXR pulses are correlated to the various radial phases of the focusing dynamics.

## III. THE RESULTS

Results are shown in Figures 3-5 and discussed.

Fig 3 shows that the computed current waveform is fitted very well to the measured current waveform, the two waveforms lying on top of each other appearing as one up to the point t=3.9 μs which is the end of the RAN phases. Fig 3 also shows the outputs of the two channels of SXR. The voltage waveform is not shown so as not to clutter Fig 3. The four measured waveforms are displayed on the same 4-channel DSO.

In Fig 3 the start and end of the computed Regular Dip RD from the 5-phase model are indicated by arrows. The anomalous resistance (RAN) regions lie past the end of the RD and extends to t=3.9 μs which is the end of the RAN region beyond which the fitting of computed and measured is stopped.

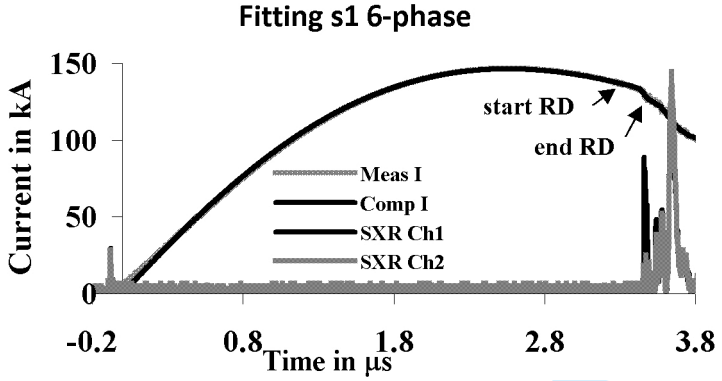


Fig 3 Correlating currents and SXR channels. The computed current is fitted so well to the measured current that the two traces overlap, appearing as one trace (the top trace). The SXR Ch1 and the SXR Ch2 also overlap very well except the first pulse (just after 3.4 μs) which is dominated by Ch1. Ch1's output is also slightly bigger than Ch2 for the second pulse; but the third pulse and very large fourth pulse (appearing just before 3.8 μs) have the outputs of Ch1 and Ch2 inseparably overlapping.

Fig 4 is an expansion of Fig 3 for the region 3.3 to 3.9 μs. It shows the outputs of the two SXR channels. From this Fig 4 we see that the first SXR straddling the pinch duration is predominantly characteristic neon SXR (since there is a difference pulse). After the pinch phase there is the short (few ns) RAN1 phase which coincides with the tail of the characteristic neon SXR pulse. The 3 RAN sub-phases are indicated by the thin 'humpy' line running across near the bottom of Fig 4. The first RAN sub-phase is of very short duration shown by the almost vertically dropping thin line just after the end of the pinch phase (just resolved in the more highly expanded Fig 5). Towards the end of the RAN2 phase there is a sharp SXR pulse with a duration of less than 10ns (see Fig 4). This pulse is harder SXR than the characteristic neon SXR lines as is evidenced by the fact that the SXR Ch1 and Ch2 have almost identical outputs over the duration of this pulse, so that the difference of the two Channels is practically zero. Then at the start RAN3 there is a similar SXR pulse of slightly higher amplitude but larger pulse duration of about 40ns. The difference of the two Channels over this pulse is also nearly zero which indicates that the photon energy of this pulse is primarily harder than the characteristic neon SXR. Finally between 3.6 to 3.7 μs the main SXR pulse of this shot is emitted with a much larger amplitude (two times bigger) and a larger duration (close to 100ns). This is the major SXR emission of this shot

and the emission is not characteristic neon SXR but is a harder SXR possibly from Bremsstrahlung coming from the fully ionized neon plasma of the type observed by others [22]

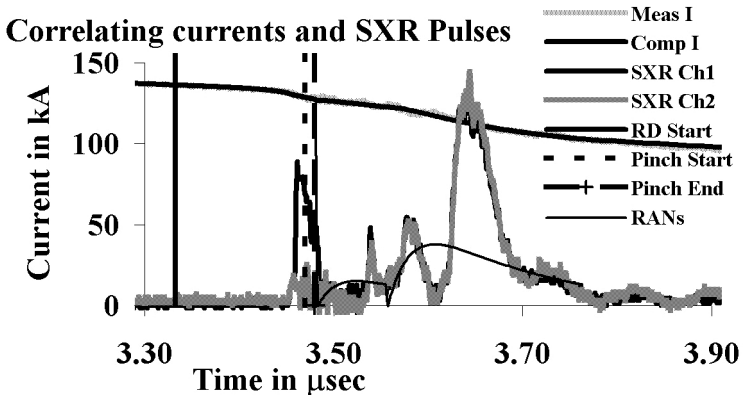


Fig 4 This is an expansion of Fig 3 from 3.3 to 3.9 μs. The top trace running across the figure is the overlapped lines of the computed and measured currents. The SXR Ch1 and Ch2 also overlap very well except the first pulse (just after 3.4 μs) which is dominated by Ch1. The 3 vertical lines are time markers for (from left) start of radial phase or RD, start of pinch phase and end of pinch phase which is also end of RD.

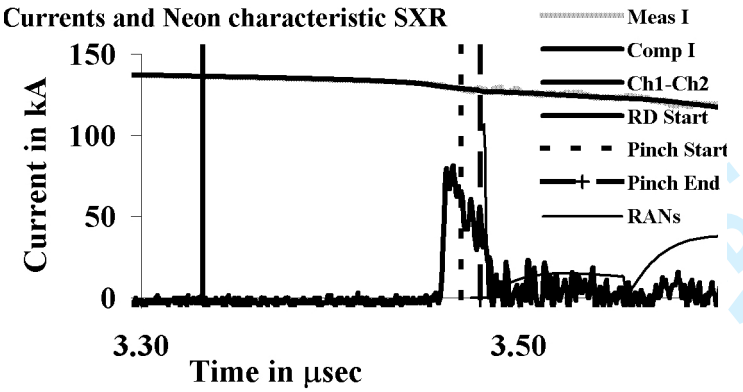


Fig 5 This is derived from Fig 4. The top trace running across the Fig 5 is the overlapped lines of the computed and measured currents. The pulse shown in this figure is the characteristic He-like and H-like neon SXR pulse obtained by subtracting Ch2 from Ch1 (see Fig 4). The 3 RAN sub-phases are indicated by the thin line running across near the bottom of Fig 5.

Fig 5 is derived from Fig 4 and shows the correlation of the measured (and computed) current with the characteristic He-like and H-like neon SXR which is the difference pulse obtained by subtracting SXR Ch2 from SXR Ch1 of Fig 4. Also shown in Fig 5 are time markers (vertical lines) indicating from the computed results the start of the radial phase (solid vertical lines), and the start and end of the focus pinch phases (dashed vertical lines). The RAN sub-phases are also indicated by the anomalous resistances (denoted by the light 'humpy' line in arbitrary units).

The results show (for this particular shot) the characteristic neon SXR starts strongly some 10 ns before the pinch phase (see Fig 5), the pulse dropping in amplitude through the 10 ns duration of the pinch phase and continues to drop to zero for another 5 ns after the pinch phase into the first anomalous resistive (RAN) phase. There is little or no characteristic neon SXR beyond this single pulse of SXR which lasts some 25 ns in total duration, straddling the 10 ns pinch phase. This characteristic He-like and H-like neon SXR pulse for this shot is integrated and found to have a radiation yield of 1.1 J.

Analysis of a number of shots at 12 kV 2 Torr neon establishes that the correlation of Figures 4 & 5 is typical of most of the shots. The characteristic neon SXR line yields of these typical shots at 12 kV 2 Torr neon lies in the range 1.0J to 1.1J. There are also a low % of shots which give higher neon yields of 3-4J. These are characterized by much wider pulses with significant contributions of characteristic neon SXR in the RAN regimes.

## IV. THE CONCLUSION

The SXR pulses emitted from the INTI PF (one of the UNU ICTP PFF series) at 12 kV, 2 Torr neon (optimum characteristic neon line yield condition) are differentiated into characteristic He-like and H-like neon line SXR within the spectral window of 900-1550 eV and other (non characteristic) neon SXR emission with photonic energy higher than 1550 eV. These SXR

emissions are carefully correlated to the time profiles of the measured and fitted computed currents. It is found that the characteristic He-like and H-like neon line SXR are emitted 10 ns before the pinch phase, achieving peak amplitude during these 10 ns, then continues to be emitted with lower amplitude through the 10 ns pinch phase, then dropping to zero amplitude over another 5 ns as the plasma goes through its first anomalous resistance RAN1. During the second RAN period there is a sharp (few ns duration) SXR pulse with only a very small amount of characteristic neon line SXR; the emission in this pulse is SXR harder than 1550 eV. During the third RAN period there are two pulses of similar non-characteristic neon SXR (harder than 1550 eV). The first of these has a duration of 40 ns occurring at the start of RAN 3 sub-phase. The second of these is the main SXR pulse for this shot with a much higher amplitude and a duration of 100 ns.

These results may be further summarized as follows: The characteristic He-like and H-like neon line SXR pulse straddles the pinch phase emitting strongly before, during and a little after the pinch phase of the focusing action. After the pinch phase follows the anomalous resistance phase during which several harder SXR pulses are emitted of primarily non-characteristic neon SXR, possibly Bremsstrahlung.

These results have implications in improving the Model code for the computation of characteristic He-like and H-like neon line SXR yield.



REFERENCES

[1] S. Lee, Radiative Dense Plasma Focus Computation Package: RADPF; http://www.intimal.edu.my/school/fas/UFLF/File1RADPF.htm and http://www.plasmafocus.net/IPFS/modelpackage/File1RADPF.htm (2010).
[2] M. Akel, S.Al-Hawat, S. H. Saw and S. Lee, "Numerical Experiments on Oxygen Soft X-Ray Emissions from Low Energy Plasma Focus Using Lee Model" *J Fusion Energy* **29** (3), 223-231 (2010).
[3] S. H. Saw, P. C. K. Lee, R. S. Rawat and S. Lee, "Optimizing UNU/ICTP PFF for neon operation" *IEEE Trans on Plasma Science* **37** (7), 1276-1282 (2009).
[4] S. Lee, P. Lee, S. H. Saw and R. S. Rawat, "Numerical Experiments on Plasma Focus Pinch Current Limitation" *Plasma Phys and Contr Fusion* **50** (6), 065012 (2008).
[5] S. Lee and S. H. Saw, "Pinch current limitation effect in plasma focus" *Appl Phys Lett* **92** (2) (2008).
[6] S. Lee "Neutron Yield Saturation in Plasma Focus-A fundamental cause" *App Phys Lett* **95** (15), 151503 (2009).
[7] S. Lee, R. S. Rawat, P. Lee and S. H. Saw, "Soft x-ray yield from NX2 plasma focus" *J Appl Phys* **106** (2), 023309 (2009).
[8] Lee S., Saw S. H., Lee P. C. K., Rawat R.S., and Schmidt H., (2008) "Computing plasma focus pinch current from total current measurement," *Appl. Phys. Lett.*, ***92***, no. 11, p. 111 501
[9] S. Lee and S. H. Saw "Neutron Scaling Laws from Numerical Experiments" *J Fusion Energy* **27**, 292-295 (2008).
[10] S. Lee "Current and Neutron Scaling for Megajoule Plasma Focus Machines" *Plasma Phys and Contr Fusion* **50** (10) (2008).
[11] Lee S., (2008) "Current and neutron scaling for megajoule plasma focus machines," *Plasma Phys. Control. Fusion*, ***50***, no. 10, p. 105 005 (14pp).
[12] S Lee, S H Saw, A E Abdou and H Torreblanca "Characterizing plasma focus devices- role of thestatic inductance- instability phase fitted by anomalous resistances" *J Fusion Energy* DOI 10.1007/s10894-010-9372-1; Published online: 25 December 2010
[13] Liu Mahe. *Soft X-rays from Compact Plasma Focus* (1996)- PhD thesis, Nanyang Technological University, Singapore
[14] S Lee, S H Saw, R S Rawat, P Lee, R Verma, A.Talebitaher, H Murtaza, A E Abdou, Mohamed Ismail, Amgad Mohamed, H Torreblanca, Sh El Hawat, M Akel, P L Chong, F Roy, A Singh, D Wong, K Devi "Pulsed Current Measurements in Plasma Focus Machines" accepted *INTI Journal*
[15] S. Lee, T. Y. Tou, S. P. Moo, M. A. Eissa, A. V. Gholap, K. H. Kwek, S. Mulyodrono, A. J. Smith, Suryadi, W. Usada, and M. Zakaullah "A simple facility for the teaching of plasma dynamics and plasma nuclear fusion" *American J Phys* - January 1988 -- Volume **56**, Issue 1, pp. 62
[16] W.Wang, A. Patran, S. Lee, and P. Lee, "Simple, effective multichannel pin diode X-ray spectrometer system," *Sing. J. Phys.*, **17**, no. 1, p.27, 2001.
[17] D. Wong, A. Patran, T. L. Tan, R. S. Rawat, and P. Lee "Soft X-ray optimization studies on a dense **plasma focus** device operated in neon and argon in repetitive mode" *IEEE Trans on Plasma Sci.* **36**, No. 6, pp 2267, 2004.
[18] Zhang Guixin. *Plasma Soft X-ray Source for Microelectronich Lithography* (1999)- PhD Thesis, Nanyang Technological University, Singapore
[19] A G Michette and C J Buckley 1993. *X-Ray Science and Technology* (Bristol: Institute of Physics Publishing) p 249
[20] Henke B L, Gullikson E M And Davis J C "X-ray interactions: photoabsorption, scattering, transmission, and reflection at E= 50-30,000 eV, Z= 1-92" At. Data Nucl. Data Tables **54** 181–342, 1993
[21] S H Saw, S Lee, F Roy, PL Chong, V Vengadeswaran, ASM Sidik, YW Leong & A Singh "In-situ determination of the static inductance and resistance of a plasma focus capacitor bank" *Rev Sci Instruments* **81**, 053505 (2010) published online 21 May 2010
[22] A. Bernard et al "Scientific Status of Plasma Focus Research" *J Moscow Physical Society* **8**, 93-170 (1998)